Bull Volcanol (2014) 76:861
DOI 10.1007/s00445-014-0861-3

RESEARCH ARTICLE

Representivity of incompletely sampled fall deposits in estimating eruption source parameters: a test using the 12–13 January 2011 lava fountain deposit from Mt. Etna volcano, Italy

Daniele Andronico · Simona Scollo · Antonio Cristaldi · Maria Deborah Lo Castro

Received: 13 September 2013 / Accepted: 23 August 2014 / Published online: 4 September 2014

Abstract The Southeast Crater (SEC) of Mt. Etna, Italy, is renowned for its high activity, mainly long-lived eruptions consisting of sequences of individual paroxysmal episodes which have produced more than 150 eruptive events since 1998. Each episode typically forms eruption columns followed by tephra fallout over distances of up to about 100 km from the vent. One of the last sequences consisted of 25 lava fountaining events, which took place between January 2011 and April 2012 from a pit-vent on the eastern flank of the SEC and built a new scoria cone renamed New Southeast Crater. The first episode on 12–13 January 2011 produced tephra fallout which was unusually dispersed toward to the South extending out over the Mediterranean Sea. The southerly deposition of tephra permitted an extensive survey at distances between ~1 and ~100 km, providing an excellent characterization of the tephra deposit. Here, we document the stratigraphy of the 12–13 January fallout deposit, draw its dispersal, and reconstruct its isopleth map. These data are then used to estimate the main eruption source parameters. The total erupted mass (TEM) was calculated by using four different methodologies which give a mean value of $1.5\pm0.4\times10^8$ kg. The mass eruption rate (MER) is $2.5\pm0.7\times10^4$ kg/s using eruption duration of 100 min. The total grain-size (TGS) distribution, peaked at −3 phi, ranges between −5 and 5 phi and has a median value of −1.4 phi. Further, for the eruption column height, we obtained respective values of 6.8–13.8 km by using the method of Carey and Sparks (1986) and 3.4± 0.3 km by using the methods of Wilson and Walker (1987), Mastin et al. (2009), and Pistolesi et al. (2011) and considering the mean value of MER from the deposit. We also evaluated the uncertainty and reliability of TEM and TGS for scenarios where the proximal and distal samples are not obtainable. This is achieved by only using a sector spanning the downwind distances between 6 and 23 km. This scenario is typical for Etna when the tephra plume is dispersed eastward, i.e., in the prevailing wind direction. Our results show that, if the analyzed deposit has poorer sample coverage than presented in this study, the TEM (3.4×10^7 kg) is 22 % than the TEM obtained from the whole deposit. The lack of the proximal (<6 km) deposit may cause more significant differences in the TGS estimations.

Keywords Mt. Etna · Lava fountain · Total erupted mass · Total grain-size · Mass eruption rate · Column height

Introduction

Mt. Etna, in Italy (Fig. 1), is one of the most studied volcanoes in the world owing to its very frequent effusive and explosive eruptions (e.g., Allard et al. 2006; Alparone et al. 2007; Andronico et al. 2013), which allow volcanologists to advance their scientific knowledge of eruptive processes. Since 1989, the volcanic activity has mostly taken place at the Southeast Crater (SEC), one of the Etna summit craters, situated about 3,200 m above sea level (hereafter m a.s.l.; Fig. 1b). This crater has produced several eruptions involving multiple eruptive episodes, defined as "episodic" eruptions by Andronico and Corsaro (2011) and similar to events at Kilauea, which are characterized by long-lived episodic activity (e.g., Parfitt and Wilson 1994). The "episodic" eruptions of Etna consist of sequences of individual, paroxysmal episodes/events. Each episode lasts a few hours and is characterized by paroxysmal explosive activity ranging from powerful Strombolian activity

Editorial responsibility: T. Thordarson

D. Andronico (✉) · S. Scollo · A. Cristaldi · M. D. Lo Castro
Istituto Nazionale di Geofisica e Vulcanologia, Osservatorio Etneo—Sezione di Catania, Piazza Roma 2, 95125 Catania, Italy
e-mail: daniele.andronico@ct.ingv.it

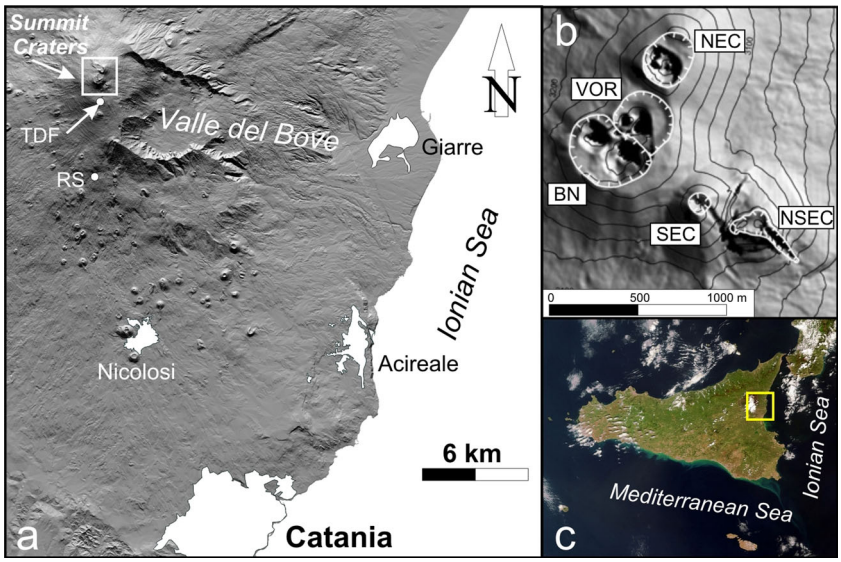

Fig. 1 **a** Map of Etna; *TDF* Torre del Filosofo; *RS* Rifugio Sapienza; **b** map of the summit craters (*white rectangular* represented in **a**) upgraded in 2013 (courtesy of INGV—Cartography Laboratory): *SEC* Southeast Crater, *NSEC* new cone formed above the 12–13 January 2011 pit-vent, *NEC* Northeast Crater, *VOR* Voragine, *BN* Bocca Nuova; **c** image of Sicily taken on 26 April 2013 from Envisat satellite (http://www.esa.int/Our_Activities/Observing_the_Earth/Envisat); *yellow rectangular* area represented in **a**

to lava fountaining (here, lava fountains are taken to be continuous gas jets propelling molten lava clots surrounded by a darker envelope of finer pyroclasts; Allard et al. 2005). These episodes produce eruption columns up to 10 km a.s.l. and associated tephra falls extending several tens of kilometers from the volcano (Alparone et al. 2007). Major recent periods of paroxysmal episodes took place in 1998–99 (23 episodes; Behncke et al. 2006), 2000 (64; Alparone et al. 2003), 2001 (15; Falsaperla et al. 2005), 2006 (18; Andronico et al. 2009a,b; 2014) and 2011–12 (25; Andronico et al. 2012; Ganci et al. 2012; Behncke et al. 2014). The last of these sequences began on 12 January 2011 from a pit-vent formed on 6 November 2010 at about 3,000 m a.s.l. in the eastern flank of the SEC (Andronico et al. 2013; Fig. 2). Here, a new flank cone (named the New Southeast Crater, hereafter NSEC) was gradually built by 25 lava fountain episodes, the last of which was on 24 April 2012. There were two other sequences in 2013, between February and April and between October and December, which featured 13 lava fountains, and another 8 paroxysmal events, respectively.

Fig. 2 The Southeast Crater as it appeared on 18 January 2011, a few days after the lava fountain episode (photo by D. Andronico); the *arrow* indicates the pit-crater degassing on its flank

Due to prevailing westerly winds (Barsotti et al. 2010; Scollo et al. 2013), tephra fall deposits from Etna are normally dispersed to the East over the Valle del Bove and the eastern flanks of the volcano. These fallout events may affect the villages situated on the medial east slope of the volcano as well as along the Ionian shoreline (Fig. 1a, c). In this eastern sector of the volcano, sample collection and mapping of the tephra deposits is confined to distances between 6–7 km and 18–26 km from the eruptive vent because the upper part of the Valle del Bove between 0 and 6 km is inaccessible, as is tephra that falls beyond the coastline. Limited exposures accessible for field survey, particularly in the proximal and distal dispersal areas, prevents a complete study of tephra deposits (Longchamp et al. 2011). Hence, this will lead to a biased assessment of physical parameters and thus can affect interpretations of eruption dynamics and behavior.

The 12–13 January 2011 event dispersed tephra to the south of the volcano and beyond the southern coastline of Sicily. This provided a rare opportunity to map, sample, and describe the fall deposit over a distance of more than 100 km. This also helps us to better define the proximal stratigraphic features and evaluate the total erupted mass (TEM) and total grain-size (TGS) distribution and to assess the column height (estimated 6 km above the vent by Calvari et al. 2011) and associated values of mass eruption rate (MER). From this data set, the representivity of the more commonly formed east-dispersed tephra fall deposit can be assessed. Based on the distribution of the available pre-2011 samples, we defined a sector of the deposit between 6 and 23 km where both TEM and TGS can be evaluated, corresponding to the region of fall deposits typically investigated on the east side of the volcano.

This study of the 12–13 January 2011 event, the first of the 2011-sequence, has therefore two objectives: (i) to characterize the explosive activity from the physical properties of the fallout deposit, and (ii) to quantify the uncertainty that results

when mapping and sampling is confined to the medial portion of the tephra fall deposit, as is a common case at Etna.

The 12–13 January 2011 lava fountain

Previous eruptive activity

The 12–13 January 2011 paroxysm was preceded by weak explosive activity from three of the four summit craters of Etna which took place throughout 2010 producing more than 30 ash emitting events, including three relatively large events that supported up to 1-km-high eruption columns (Andronico et al. 2013). A few weeks earlier, the pit-crater on the SEC slope was discontinuously active, producing night glow, profound rumbling and ash emissions. On 29–30 December 2010, intermittent glow preceded the resumption of weak Strombolian explosions, which were confined to the pit-crater and took place between 2 and 3 January 2011 and then again in the evening of 11 January. A complete chronology of the activity leading up to the 12–13 January lava fountain is provided by Calvari et al. (2011) using real-time recordings from the video-surveillance system of Istituto Nazionale di Geofisica e Vulcanologia, Osservatorio Etneo (INGV-OE), which consisted at that time of five visible and two thermal cameras. For the purposes of this paper, we briefly refer to the three main eruptive phases defined by Alparone et al. (2003). *Resumption phase* is characterized by the beginning of explosive phenomena. This phase is typified by steadily increasing intensity of Strombolian explosive activity that leads to intensifying lava fountaining, which in turn culminates in the *paroxysmal phase* featuring a sustained eruption column. The *conclusive phase* is the final part of the lava fountaining episode characterized by a steady decline in intensity and eventual termination of lava fountaining.

Chronology

The Strombolian activity (*resumption phase*) started on 11 January. The activity continued into the next day with a steady increase in explosion frequency and intensity after 18:00 GMT, when incandescent bombs began to be ejected from the pit, while in the evening a lava flow was erupted from the pit-vent. After 21:40 GMT of 12 January, pulsating lava fountains (100–200 m high) emerged from the primordial NSEC, changing at about 21:50 GMT to continuous fountaining activity (up to ~800 m high) supporting a sustained eruption column. This change demarcated the transition to the *paroxysmal phase*. Examinations using the video-surveillance system showed that the eruption plume was at 9 km a.s.l. (Calvari et al. 2011). Video-recordings show that the eruption intensity began to drop at ~23:15 GMT, to such a degree that by ~23:30 it did not support a sustained eruption plume. Both effusive and explosive phenomena completely ceased after 04:15 GMT (*conclusive phase*).

Methods

The 12–13 January 2011 tephra fall deposit, one of the few that has been dispersed to the south, was surveyed and sampled from 13 to 18 January. Based on thickness/mass per unit area and grain-size features of the fall deposit, the outcrops downwind from the vent were categorized as proximal, medial, distal and very distal, corresponding to distances from the SEC of 0 to 1–2 km, 1–2 to 5–6 km, 5–6 to 20–25 km, and more than 20–25 km, respectively (see below "Results" section). The term *scoria* is used to indicate tephra clasts commonly erupted during lava fountaining at Etna as lapilli and bombs and characterized by a vesicularity spanning the range 0.53–0.74 (Polacci et al. 2006).

Sampling was carried out along the entire length of the tephra fall deposit, from the vents to the Mediterranean coast of Sicily (Fig. 1c). In total, 45 samples were collected between Torre del Filosofo (TDF; 2,920 m a.s.l.), located 1 km and Modica (416 m a.s.l.) 103 km south of the pit-vent (Fig. 1). Measurements of tephra load per unit area were also carried out and used to construct an isomass map (i.e. the mass of deposit/m^2) (Table 1). In the case of the 12–13 January lava fountain, we were able to obtain thickness measurements for the proximal deposit in five sites. An additional 15 samples were collected 0.7-12 km from the source vent. These samples were collected on selected surfaces with sufficiently large horizontal dimensions to make the sampling statistically representative with respect to grain-size. These sampling areas ranged from 10 to 100 m^2, over which 10 largest clasts were collected for measurement of the maximum clast dimension (Md). Tephra samples were first oven-dried at a temperature of 110 °C and then weighed before analysis in the Sedimentology and Optic Microscopy Laboratory of INGV-OE. Large (>1 kg) samples were divided by Retsch RT 6.5 and RT 75 splitters until we obtained sample sizes representative and suitable for analysis. Grain-size measurements were carried out at 1 phi intervals, with phi the $-\log_2 d$, where d is the particle diameter in millimeters. This was carried out by mechanical sieving (via a Retsch Vibratory Sieve Shaker AS 200 Basic) for samples containing larger than 0.8 mm (greater than −3 phi) particles, and by CAMSIZER (Retsch) for the size fraction below this size limit. The CAMSIZER has measurement limits 0.030–30 mm (Lo Castro and Andronico 2008). When calculating the grain-size distribution, constant density is assumed for the measured particles. The mechanical sieving and the CAMSIZER measurements have a size bin overlap of 9 phi. Calibration tests using the Xcmin (the shortest chord of the measured set of maximum chords of a

Table 1 List of samples with associated locations, UTM coordinates, weight per square meter, and the main grain-size parameters of the collected samples (median, σ, F1 and F2). Median and σ have been calculated following Folk and Ward (1957), while F1 and F2 (% of particles with dimension less than 1 and 0.063 mm, respectively) are derived by Walker (1971)

Sample	Location	X (UTM)	Y (UTM)	Weight	Mdφ	σ	F1	F2
1	Belpasso SS92	37° 38′ 44.98″ N	14° 59′ 41.03″ E	237.02	0	0.7	90.4	0.1
2	Piano Vetore	37° 41′ 20.97″ N	14° 58′ 39.71″ E	133.89	0	1.7	62.9	0.5
3	Rifugio Sapienza	37° 42′ 3.76″ N	14° 59′ 57.09″ E	1082.77	−1.3	1.2	40.0	0.2
4	Torre del Filosofo	37° 44′ 16.55″ N	15° 0′ 1.57″ E	63542.44	−2.8	1.3	12.4	0.7
5	Funivia	37° 43′ 5.73″ N	14° 59′ 58.92″ E	1996.97	−2.1	1.3	21.1	0.3
6	La Quercia1	37° 40′ 9.71″ N	14° 59′ 13.58″ E	286.43	0	0.8	85.9	0.4
7	Nicolosi	37° 37′ 43.58″ N	15° 0′ 29.86″ E	23.39	0.4	0.6	98.8	0.0
8	Monte dei Santi	37° 41′ 41.25″ N	14° 58′ 9.39″ E	28.35	−3.4	0.8	0.0	0.0
9	Baita (m 2125)	37° 42′ 22.08″ N	14° 59′ 41.11″ E	2732.97	−0.8	1.2	54.5	0.2
10	Pilone Funivia (m 2125)	37° 42′ 31.54″ N	14° 59′ 55.90″ E	1488.56	−1.2	1.2	43.1	0.2
11	Montagnola (m 2615)	37° 43′ 3.08″ N	15° 0′ 23.37″ E	963.83	–	–	–	–
12	Shelter (m 2600)	37° 43′ 7.99″ N	15° 0′ 15.45″ E	1815.58	−1.2	1.8	14.4	0.6
13	Seismic Station (m 2940)	37° 44′ 20.58″ N	14° 59′ 50.65″ E	30540.94	−3.2	1.5	6.2	0.4
14	2006 Bocca Nuova lava flow	37° 44′ 28.88″ N	14° 59′ 30.82″ E	2807.06	−3.6	1.3	6.8	0.5
15	Intermediate summit site	37° 44′ 25.59″ N	14° 59′ 38.89″ E	20242.81	−2.8	1.4	12.5	0.7
16	2002-03 lava flow	37° 43′ 34.14″ N	15° 0′ 13.56″ E	3310.13	−3.1	1.4	7.2	0.6
17	Agip	37° 28′ 51.59″ N	15° 0′ 43.14″ E	0.06	1.7	1.4	98.9	8.4
18	Motta	37° 30′ 46.50″ N	14° 57′ 40.06″ E	31.32	0.4	0.6	99.7	0.5
19	Aeroporto	37° 28′ 18.66″ N	15° 4′ 7.66″ E	0.03	–	–	–	–
20	Gelso Bianco	37° 27′ 43.67″ N	15° 0′ 26.42″ E	0.06	–	–	–	–
21	Motta 2	37° 28′ 19.78″ N	14° 56′ 24.18″ E	35.68	0.5	0.6	99.9	0.0
22	Sferro	37° 30′ 3.39″ N	14° 47′ 51.20″ E	0.05	–	–	–	–
23	Etnapolis 1	37° 32′ 50.36″ N	14° 57′ 0.63″ E	69.95	0.1	0.5	97.7	0.1
24	Etnapolis 2	37° 32′ 47.86″ N	14° 56′ 52.83″ E	89.58	0	0.6	97.2	0.1
25	Paternò	37° 34′ 30.87″ N	14° 54′ 42.14″ E	1.82	1.5	1.0	98.4	0.5
26	Belpasso	37° 35′ 25.86″ N	14° 58′ 38.79″ E	90.00	−0.3	0.6	91.3	0.1
27	Borrello	37° 36′ 6.77″ N	14° 59′ 6.99″ E	126.86	−0.4	0.6	86.1	0.2
28	Contrada S. Leo	37° 38′ 44.43″ N	14° 59′ 16.50″ E	332.52	−0.9	0.8	54.9	0.0
29	Piano Bottara	37° 40′ 11.57″ N	14° 59′ 15.31″ E	524.80	−1.5	1.0	30.3	0.0
30	Ragalna	37° 38′ 43.11″ N	14° 57′ 37.33″ E	33.19	−1.5	1.5	32.2	0.0
31	Ragalna Municipio	37° 38′ 4.95″ N	14° 56′ 36.83″ E	9.92	−1.8	1.0	15.9	0.1
32	Ragalna lower town	37° 38′ 2.51″ N	14° 54′ 40.46″ E	0.89	1.5	0.6	98.2	0.7
33	Piano Tavola exit	37° 32′ 30.12″ N	14° 58′ 38.96″ E	36.32	0.3	0.7	99.2	1.2
34	Piano Tavola	37° 32′ 2.19″ N	14° 59′ 21.04″ E	6.78	0.3	0.5	99.6	0.0
35	SS385	37° 19′ 52.62″ N	14° 48′ 36.06″ E	0.33	1.7	0.7	99.9	1.2
36	Militello road	37° 18′ 47.96″ N	14° 48′ 39.74″ E	1.17	2	0.5	100.0	2.1
37	Militello	37° 16′ 32.99″ N	14° 48′ 3.60″ E	0.74	2	0.8	99.8	5.2
38	Vizzini Scalo	37° 10′ 59.28″ N	14° 43′ 44.28″ E	0.35	2.1	0.8	99.7	3.9
39	Licodia Eubea	37° 9′ 40.29″ N	14° 42′ 36.74″ E	0.64	–	–	–	–
40	Francofonte 1	37° 13′ 33.36″ N	14° 53′ 17.63″ E	9.66	1.6	0.6	100.0	3.2
41	Francofonte 2	37° 13′ 36.57″ N	14° 50′ 51.98″ E	8.24	–	–	–	–
42	Buccheri	37° 7′ 27.30″ N	14° 51′ 30.81″ E	13.05	–	–	–	–
43	Giarratana	37° 2′ 53.68″ N	14° 47′ 54.75″ E	12.58	1.9	0.6	100.0	6.3
44	Ragusa	36° 54′ 59.48″ N	14° 43′ 45.33″ E	2.66	1.8	0.9	99.8	3.5
45	Modica	36° 49′ 38.39″ N	14° 47′ 11.98″ E	4.81	2	0.5	100.0	2.7

Mdφ value of the median of the grain-size distribution as defined by Inman (1952) and Folk and Ward (1957)

σ: sorting as defined by Folk and Ward (1957); F1 and F2 as defined by Walker (1971)

particle projection) method to calculate the particle diameter obtained via the CAMSIZER (Lo Castro, personal communication, 2014), shows that the size bins used for splicing the data from these two methods exhibit a good match, ensuring compatibility between the results of these two different techniques of grain-size analysis. Four different methods were applied to estimate the TEM, all of which are based on fitting a curve to the observed thickness versus area relationships for the fall deposit. The methods used are the straight line exponential fit of Pyle (1989), the two-segment fit of Fierstein and Nathenson (1992), the power law fit of Bonadonna and Houghton (2005) and the Weibull distribution used by Bonadonna and Costa (2012). The TGS was obtained by the Voronoi method (Bonadonna and Houghton 2005).

The average of measurements on the largest clasts at each site is used to construct the isopleth map. We have tested several averaging techniques for obtaining representative largest clast values for constructing the isopleth map. Considering that at Etna the fall deposits from lava fountaining activity typically do not contain many lithic fragments (and they are indeed largely absent as in the 12–13 January deposit), we are forced to use the juvenile clast population for these measurements. If the sampling at any one site provides "oversize" clasts (i.e., size outliers; Bonadonna et al. 2013) with dimensions >1 cm, we use measurements of the largest scoria grains in the average calculations. Using a digital caliper (Melchioni, measuring range 0–300 mm), we first measured the three orthogonal axes of the five largest clasts for each sample, and then took the largest axis of each clast and averaged them for both the three and five largest clasts. Based on the values obtained from these calculations, we opted to use the average of the largest axis for the three largest clasts (Barberi et al. 1995). An independent estimate of the plume height was obtained through the measurement of the largest clasts via application of the Carey and Sparks (1986) method.

Dispersal, mass, and stratigraphic features of the fallout deposit

The volcanic plume formed during lava fountaining was dispersed towards the SSW, causing fallout of coarse lapilli onto the upper slopes of Etna (~1 km from the vent) and of lapilli- to ash-sized clasts further away from the volcano. Tephra fallout was confined to the area between the villages of Sferro and Licodia Eubea on its western side, and Misterbianco and Pozzallo on the east side (Fig. 3). Approaching the SEC, the fall deposit was easy to detect because it lay directly on the snow formed a few days before the 11–13 January activity. Further, the tephra fall formed a smaller internal area where the deposit was continuous; in the following, we refer to this as the Central Strip (hereafter CS). Down the axis of fall dispersal, the CS ended close to the limit

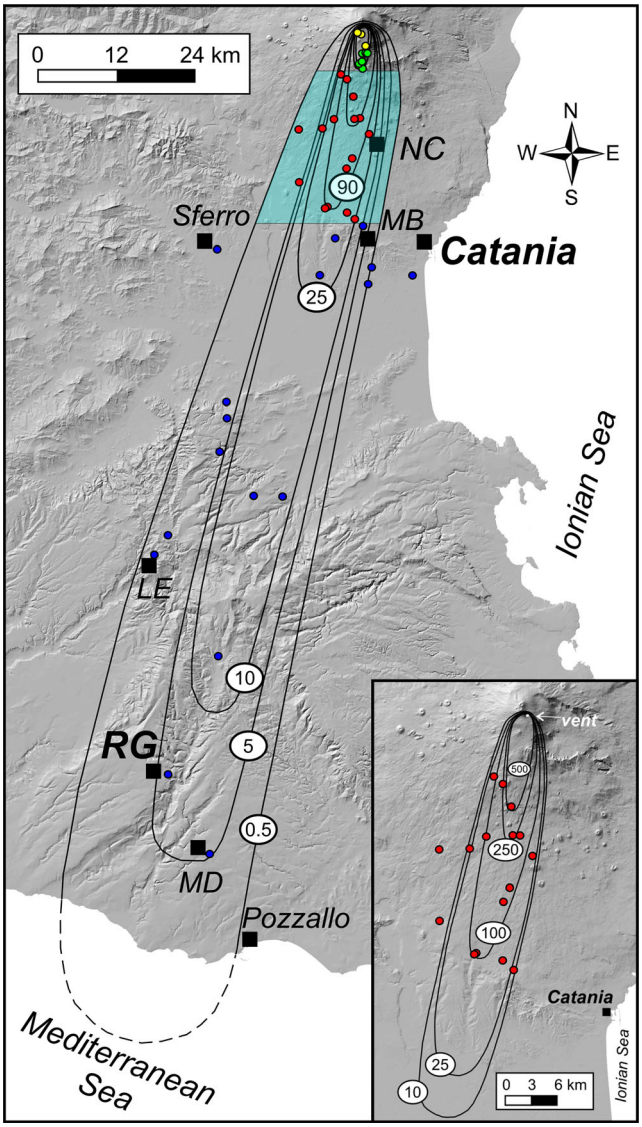

Fig. 3 Isomass map of the 12–13 January 2011 fall deposit. The isomass isolines are in grams per square meter, with *dashed line* interpolated over the sea; the values of the proximal lines (250, 1,000, 2,700, 30,000, and 60,000 g/m^2) are not reported to avoid illegibility. *Full colored circles* are sample sites; *yellow* proximal; *green* medial; *red* distal; *blue* very distal. *Full black squares* are the main towns reported in the text; *NC* Nicolosi, *MB* Misterbianco, *LE* Licodia Eubea, *RG* Ragalna, *MD* Modica. Translucent blue area indicates the intermediate sector 6–23 km from the SEC. *Inset in right bottom* isomass map of the intermediate deposit, represented by only 17 samples collected between 6 and 23 km of the 12–13 January 2011 whole deposit

between the medial and distal outcrops, at ~10 km from the vent. The rapid decay in terms of mass loading made the CS not easily traceable laterally in the medial and distal areas; in the proximal area, conversely, the coarser-grained and more abundant black deposit permitted us to define the exact lateral extent of this layer on the snow. In Fig. 4, we reported the grain-size distribution of selected samples, showing their clear decreasing in size and better sorting with distance from the vent.

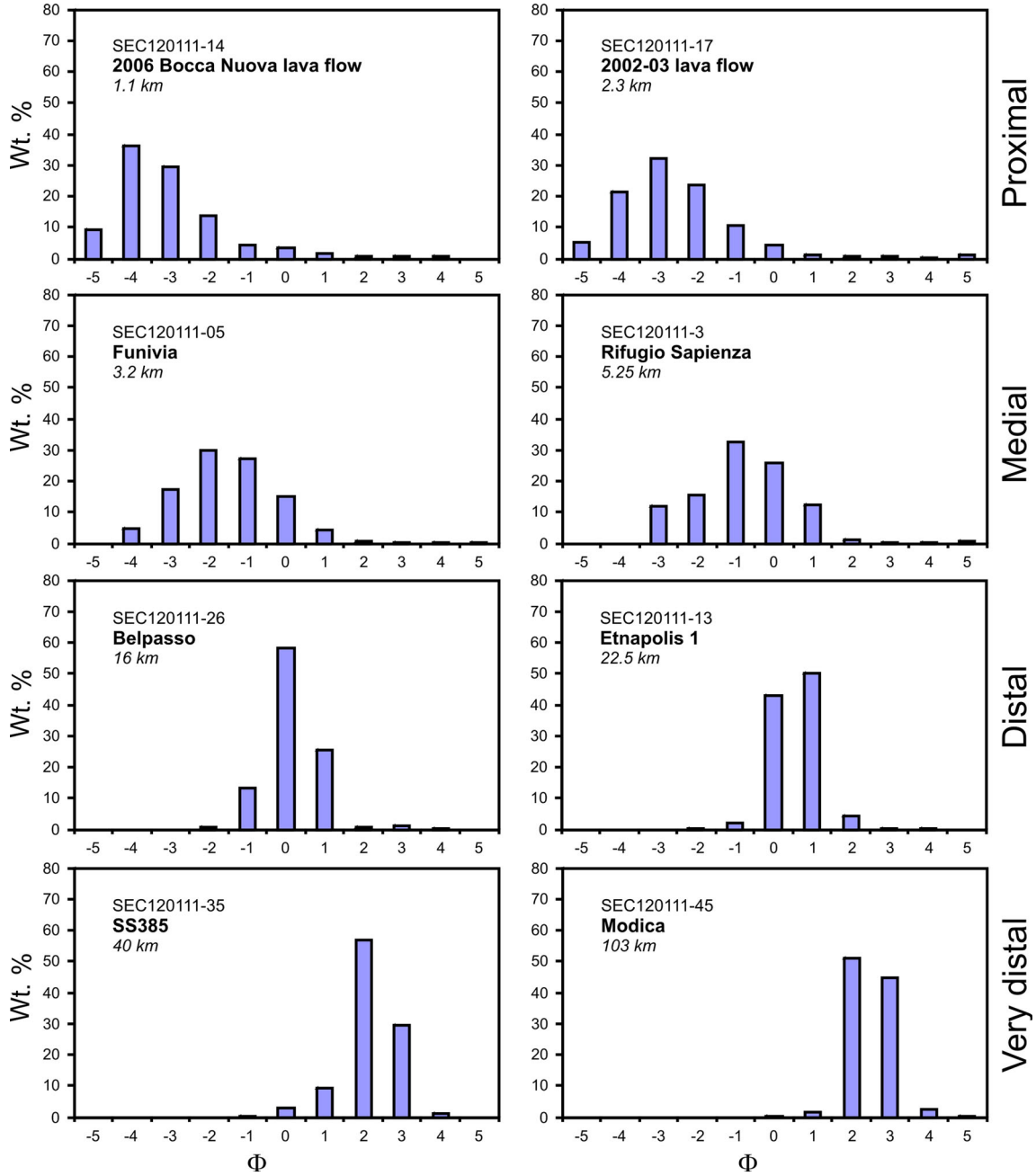

Fig. 4 Grain-size distributions of selected samples, ordered from proximal to very distal. Sample labels, sites, and distance from the vent are indicated

In the proximal deposit (up to distance of 2 km) the tephra fall formed in the CS a continuous blanket and consisted of shiny black, 1–5 cm lapilli-size scoria, mixed with scattered decimeter-outsized scoria bombs (Fig. 5a) and red-oxidized centimeter-size lapilli. The maximum thickness (20 cm; Fig. 6a) was measured at TDF (Fig. 1). Here, a thin, 3 cm thick, basal fine lapilli layer (Opening Unit) was overlain by a bed of medium size lapilli (Main Unit; Fig. 5b), which contained scattered scoria bombs up to 20 cm. Perpendicular to the dispersal axis, the Main Unit thinned to 3 cm (Fig. 6b), before changing to a discontinuous tephra carpet at about 0.9 km distance from the dispersal axis (Fig. 6c) and then passing abruptly at ~1.2 km into a region of dispersed, coarse lapilli and bomb deposits (Fig. 6d). Conversely, the Opening Unit exhibited less pronounced thinning than the Main Unit (to 1 cm; Fig. 6b), showing a sub-circular dispersal area before becoming absent at distances beyond ~1 km from the vent. The marked variation in the grain-size distribution of the Opening Unit, together with its low thickness and limited extent, are congruent with a deposit related to lower intensity fallout due to frequent, highly explosive Strombolian bursts occurring during the *resumption phase*. On the whole, the

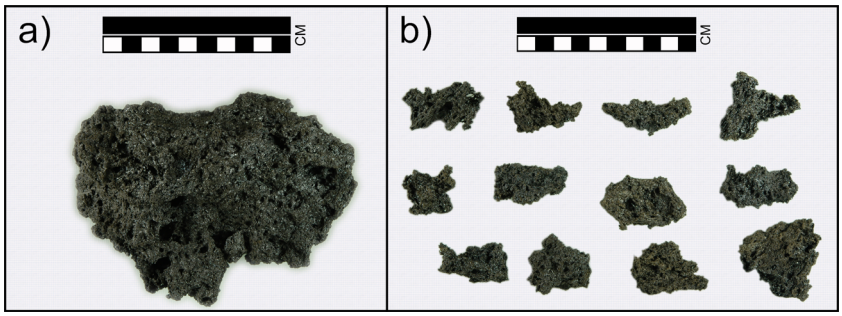

Fig. 5 Images representative of measured largest juvenile clasts from the 12–13 January 2011 tephra fallout deposit: **a** decimetric-bomb with typical scoria texture and up to centimetric bubbles on surface; **b** vesicular lapilli with sub-angular to irregular shapes

Main Unit was a poorly sorted, massive layer without apparent internal stratification in any of the studied sites. The total deposit (Opening plus Main Units) mass loading over the CS ranged from 64,000 to 20,000 g/m^2. Unfortunately, following the survey in the summit it was impossible to reach this area again and sample the Opening and the Main Units separately, because several meters of snow and other tephra fall deposits had covered the 12–13 January deposit.

The tephra fall deposit in the medial sector was significantly thinner and finer grained than in the proximal area. Within the CS, it consisted of a continuous millimeter- to centimeter-thick tephra layer composed of medium (or fine) lapilli and containing scattered coarse lapilli to decimetric scoria; the mass loading ranged between ~3,300 and ~1,000 g/m^2. The tourist area of Rifugio Sapienza (RS; Fig. 1), located at ~5 km from the vent, was covered by ~1,000 g/m^2 of fine lapilli (~48 wt.% of the mass between 2 and 4 mm) and scattered coarse lapilli grains (up to 4–5 cm of diameter) (Fig. 6e).

The distal deposit was characterized by a thin (<1 cm thick) continuous to discontinuous, relatively well-sorted ash to fine lapilli (Fig 6f). The load per square meter ranged from ~500 to

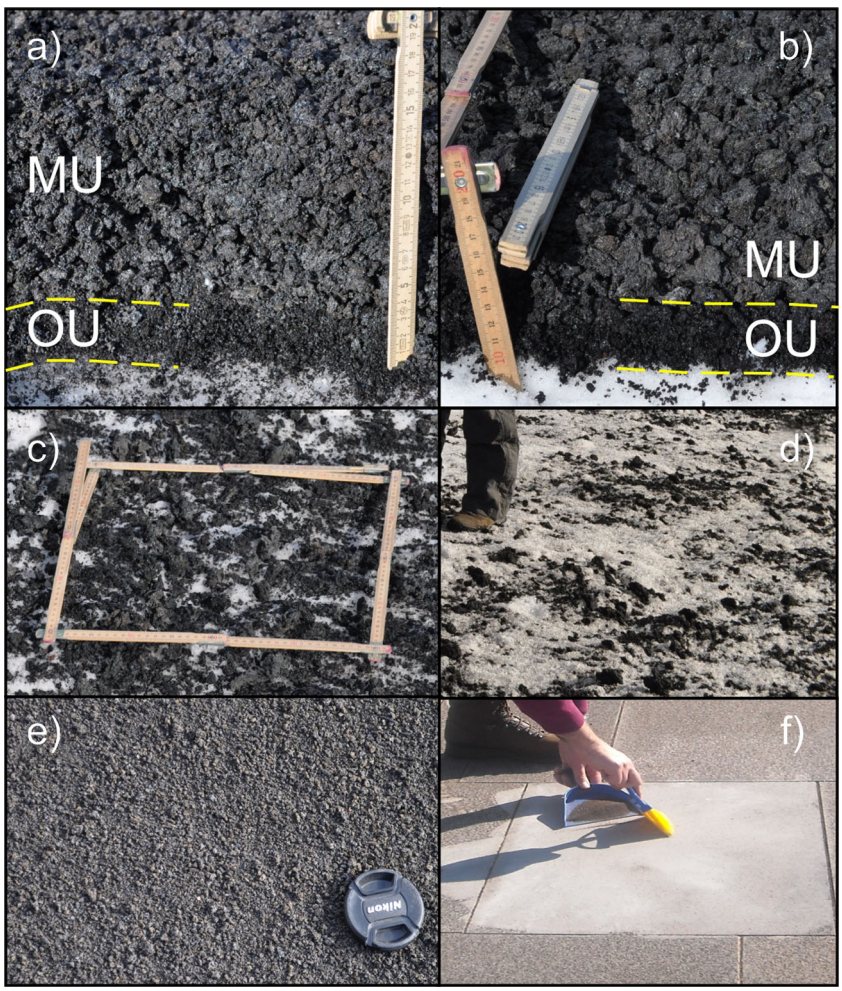

Fig. 6 Stratigraphic features of the tephra fall deposit (outcrops **a**, **b**, **c**, **d**: proximal; **e**: medial; **f**: distal). **a** TDF section; **b** BN seismic station; **c** outcrop intermediate between TDF and the border of the dispersal (*bar* size: 40×40 cm); **d** lateral outcrop. In **a**–**b** the two different units are indicated (*OU* Opening Unit; *MU* Main Unit); **e** the continuous layer of lapilli at Rifugio Sapienza; **f** discontinuous ash deposit sampled at Etnapolis. Photos **a**–**e** D. Andronico; **f** S. Scollo

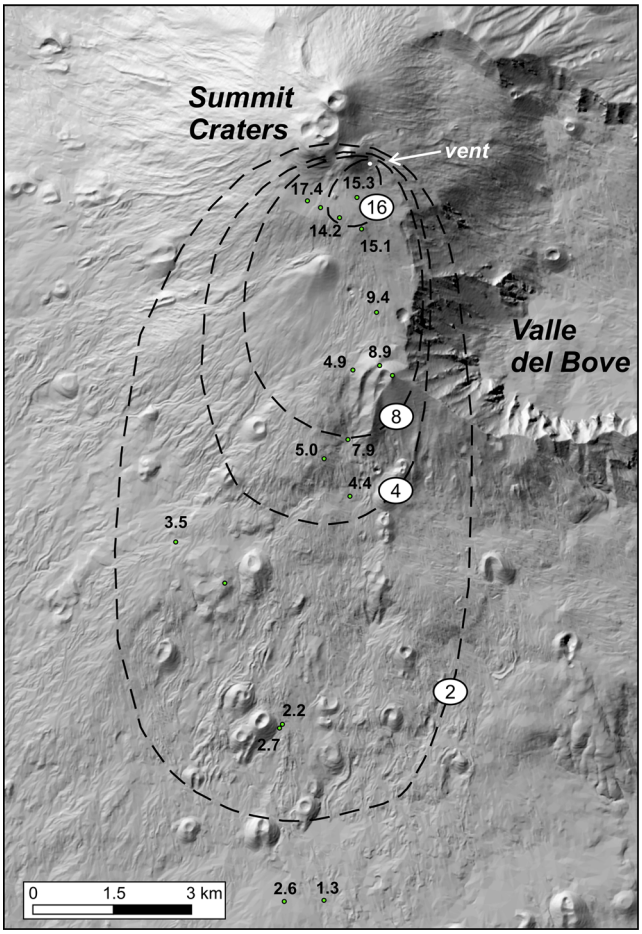

Fig. 7 Isopleth map of the 12–13 January 2011 fallout deposit to 12 km from the vent. Isolines (values in centimeters) are interpolated from 15 sites; for each site the value is the mean of the longest axes of the three largest clasts

~70 g in the CS, to a few grams at sites along the outer margins of the fallout.

In the very distal sector, the cover was more like a dusting of fine to medium ash (0.125-0.5 mm), with loading per square meter ranging from about one gram at the deposit margins to 30 g.

The tephra deposit was distributed on the ground symmetrically with respect to the main dispersal axis due to winds blowing with almost constant direction (from the NNE) and intensity (16, 15, 86, and 95 knots, at 3, 5, 7, and 9 km a.s.l.) (http://weather.uwyo.edu/). The isomass lines of the deposit are elongate and define a narrow tephra dispersal sector (Fig. 3). This is in good agreement with the intensity of the wind speed at the altitude of 7 and 9 km a.s.l. The isomass map shows that most of the erupted tephra fell within 5 km from the vent. Beyond the medial sector, the deposit load is markedly reduced, although the fallout extended to more than 100 km from the vent.

The isopleth map (Fig. 7) is broadly consistent with the isomass map (Fig. 3). Similarly to the isomass map, the size of the largest clasts drops sharply at 5 km away from the SEC and more gradually thereafter (Fig. 7).

Physical parameters

Total erupted mass

The total erupted mass (TEM) (related to total volume) is an important eruption parameter because it allows inference of the magnitude of an event (Newhall and Self 1982). However, obtaining an accurate estimate of TEM is not an easy task because of the nonlinear relation between thickness/mass and area, which is commonly further hampered by lack of adequate data particularly in the proximal and distal sectors (Bonadonna and Houghton 2005). The methods by Pyle (1989) and its extended version (Fierstein and Nathenson 1992) assume that the thinning versus area relationship is exponential, and usually display semilog plots of thickness (or mass/area) versus square root of isopach (isomass) area. These methods rely on the choice of straight segments and could underestimate the total volume/mass especially when the distal data are lacking (Fierstein and Nathenson 1992; Pyle 1989, 1995; Rose 1993). For this reason, Bonadonna and Houghton (2005) used a power law curve for estimating the total volume/mass which should give better results. However, the power law curve cannot be integrated between zero and infinity and requires that extremes of integration must be chosen a priori (Bonadonna and Costa 2012). Furthermore, these authors recently proposed a new and simpler strategy based on the integration of the Weibull function, demonstrating that it reproduces the gradual thinning of tephra deposit and does not depend on the choice of arbitrary segments or of arbitrary extremes of integration.

All these methods were applied to the 12–13 January 2011 field data providing different TEM values (Table 2). In particular, we obtained 1.64, 1.18, 1.06, 2.07×10^8 kg using the methods of Pyle (1989), Fierstein and Nathenson (1992), Bonadonna and Houghton (2005) and Bonadonna and Costa (2012), respectively (Table 2). The mean TEM value is $1.5\pm0.4\times10^8$ kg and the corresponding mean MER (considering 100 min of *paroxysmal phase* duration as constrained by video-recordings) is $2.5\pm0.7\times10^4$ kg/s. An error of 10 % associated with the compilation of isomass maps was also added on the basis of work of Biass and Bonadonna (2011). Our estimations are in good agreement with comparisons of volume calculated using different methods reported in Bonadonna and Costa (2012).

Total grain-size distribution

There are only a few published data sets on the total deposit grain-size distribution for tephra fall deposits. A likely

Table 2 Total erupted mass (TEM) and mass eruption rate (MER) estimated by different methods for the *whole* 12–13 January fall *deposit* and the *intermediate deposit* comprising only samples collected 6–23 km from the vent

Method	Fitting parameters	Whole deposit		Intermediate deposit	
	km	TEM kg	MER kg/s	TEM kg	MER kg/s
1-segment exponential[a]	b_t=1.85	1.64×10^8	2.7×10^4	3.05×10^7	5.1×10^3
2-segments exponential[b]	b_{tprox}=0.35–b_{tdist}=3.18	1.18×10^8	2.0×10^4	5.58×10^7	9.3×10^3
Power law[c]	$A^{1/2}{}_{prox}$=0.30–$A^{1/2}{}_{out}$=200	1.06×10^8	1.8×10^4	2.14×10^7	1.3×10^4
Weibull distribution[d]		2.07×10^8	3.5×10^4	2.81×10^7	4.7×10^3
Mean value		$1.5\pm0.4\times10^8$	$2.5\pm0.7\times10^4$	$3.4\pm1.3\times10^7$	$5.7\pm2.3\times10^3$

b_{tprox} and b_{tdist} proximal and distal b_t values, respectively; $A^{1/2}{}_{prox}$ and $A^{1/2}{}_{out}$ proximal and outer integration limits, respectively

[a] Pyle (1989)

[b] Fierstein and Nathenson (1992)

[c] Bonadonna and Houghton (2005)

[d] Bonadonna and Costa (2012)

explanation is that in most of the eruptions the deposit in proximal and distal sectors is poorly exposed making any attempt to calculate TGS distributions very difficult. Furthermore, there is no standard approach used by the volcanological community, making the comparison among TGSs of different deposits very difficult. Among the different methods, the statistical Voronoi method has been successfully applied to evaluate the TGS from the 1996 eruption at Ruapheu in New Zealand (Bonadonna and Houghton 2005; http://dbstr.ct.ingv.it/iavcei); it was applied to the 12–13 January 2011 deposit and also to previous Etna tephra fall deposits (e.g., 2001 and 2002–03 eruptions, 16 November 2006, 24 November 2006 and 4–5 September 2007 paroxysms; Scollo et al. 2007; Andronico et al. 2008a, b, 2009a, 2014). However, this is the first time that the TGS reconstruction may be considered complete, because the analyzed samples are representative of the full extent of the fall deposit, from proximal to very distal sites. In the previous cases, sampling of proximal-medial deposits was limited or absent, and the TGS should be taken with caution.

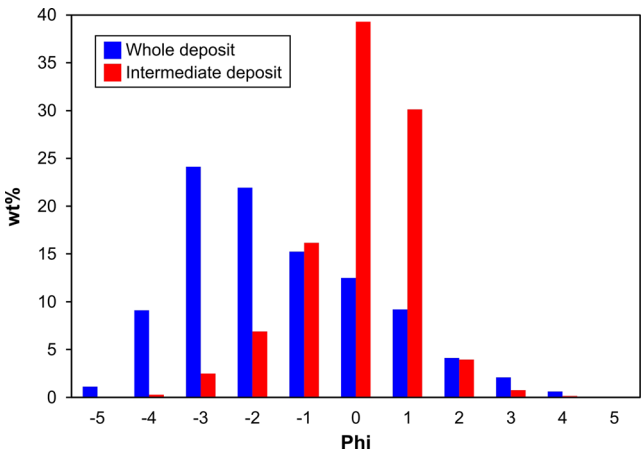

Fig. 8 The total grain-size distribution (TGS) based on the samples covering the whole dispersal area, versus "intermediate" samples only from medial sites 6–23 km from the vent

The single 12–13 January 2011 samples show grain-size distributions which range between −5 and 5 phi (Fig. 4 and Table 1). In particular, samples from proximal and medial sites (i.e., collected within 5 km from the vent) are coarser, with median grain-size ranging between −3.6 and −0.8 phi. Samples collected at distances >20 km have an almost unimodal distribution and mode at >0 phi. The TGS, estimated using 38 samples, exhibits a positively skewed distribution that has a peak value at −3 phi and a median at −1.4 phi (Fig. 8).

Column height

During the eruption, visual observations by volcanologists of the plume height were not carried out because the lava fountaining occurred in the night. We estimated the column height (Carey and Sparks 1986) by measuring the maximum downwind and crosswind ranges (Table 3) of isopleths and using a density value of 1,000 kg/m^3 (mean value from laboratory-measured clast densities ranging from 900 to 1,100 kg/m^3). Results suggest that the column height ranged

Table 3 Maximum distances used in the plots by Carey and Sparks (1986) of the crosswind range versus the downwind range for clast size of 16.0, 8.0, 4.0 and 2.0 cm in diameter with a density of 1,000 kg/m^3

Diameter cm	Maximum downwind Range m	Maximum crosswind Range m
16.0	1,125	420
8.0	5,000	1,700
4.0	6,800	2,100
2.0	12,300	3,300

Table 4 Eruption column heights (above the vent) estimated by the Carey and Sparks (1986) method

Clast diameter cm	Column height km	Wind speed m/s
16	$<<13.8$	10
8	$6.8<h<<13.8$	20
4	$6.8<<h<13.8$	20
2	13.8	30

between 6.8 and 13.8 km above the vent (Table 4). It is worth highlighting that these values must be considered as the minimum and maximum estimates for the column height. Wind speed is comparable with that measured by the radiosounding (http://weather.uwyo.edu/).

We also estimated the column height using the Wilson and Walker (1987) equation and their modified version for an eruption temperature of 1,300 K (Pistolesi et al. 2011) and the Mastin et al. (2009) equation with the value of the MER estimated by the deposit characteristics (see section "Total mass") (Table 5). The estimated column height using this value of MER (i.e., 2.5×10^4 kg/s) is much lower, 3.4± 0.3 km above the vent (Table 5).

Uncertainty in TEM and TGS resulting from unsampled proximal and distal deposits

In order to assess the uncertainty that arises in many studies which lack proximal and distal data when deposits are dispersed to the East of Etna with prevailing wind conditions, we evaluated the TEM and TGS of an *intermediate deposit* represented by only 17 samples collected between 6 and 23 km of the *whole deposit*, a spatial range which represents well the accessible area on the Etna eastern flank. The isomass map of the hypothetical *intermediate deposit* consists of five different isomass lines of 10, 25, 100, 250, and 500 g/m^2 (Fig. 3). The new analysis shows that the TEM is between 14 and 47 % of TEM found by analyzing the whole set of samples (Table 2); the greatest difference is with the Pyle and Weibull methods.

The same samples were used to evaluate again the TGS. In this case, the TGS of the hypothetical *intermediate deposit* is peaked at 0 phi (mode) and has a median value of 0.5 phi (Fig. 8). These values differ by about 3 phi and 2 phi for the mode (−3 phi) and median (−1.4 phi), respectively, from the true TGS.

Table 5 Comparison between column height (CH; values above the vent) and mass eruption rate (MER) calculated using different methods (eruption duration of 100 min); the arrows indicate how column height or MER was calculated

Method	Column height km		MER kg/s
INGV-camera network	6±1.2[a]	→	$1.7\pm1.3\times10^{5}$[b]
MER-CH relationship	3.4±0.3[c]	←	$2.5\pm0.7\times10^{4}$[d]
Maximum clast	6.8±1.3<CH <13.8±2.8[e]	→	$1.2\times105–6.9\times10^{6}$[f]

$CH1=0.295\times MER^{0.25}$ (Pistolesi et al. 2011), $CH2=0.236\times MER^{0.25}$ (Wilson and Walker 1987), $CH3=0.3035\times MER^{0.241}$ (Mastin et al. 2009)

[a] Value of CH from Calvari et al. (2011) affected by an uncertainty of 20 % from Scollo et al. (2008)

[b] MER from Pistolesi et al. (2011)

[c] Mean [CH1, CH2, CH3]

[d] Mean value of MER from the deposit

[e] CH obtained by Carey and Sparks (1986)

[f] Minimum and maximum values of MER obtained by Pistolesi et al. (2011)

Discussion

Stratigraphic features and dispersal of the tephra fall deposit

The eruption dynamics of the 12–13 January 2011 paroxysm were recorded by dispersal features and physical properties of the tephra fall deposit, which consists of two stratigraphic units. In very proximal outcrops, we found a 1–3-cm-thick basal layer (Opening Unit) composed of fine lapilli related to the *resumption phase*. This layer was extremely weakly dispersed and thus rather small in terms of mass/volume compared with the main, invariably overlying, coarse scoria deposit (Main Unit). Therefore, the contribution of the Opening Unit is volumetrically negligible and its presence does not significantly influence the TEM and TGS values.

The Main Unit is a widely dispersed deposit and was produced by the eruption column which formed during the lava fountaining activity, i.e. the *paroxysmal phase*. It can be traced as a unique layer from the proximal to the very distal outcrops, i.e. over a distance of more than 100 km. Although recording a single eruptive phase, dispersal data, mass per unit area and grain-size of the 12–13 January tephra fallout deposit show significant variations with distance from the eruptive vent. Such variations can be suitably correlated and used to infer the eruptive processes taking place during the lava fountaining.

In the proximal and the medial sites, the Main Unit, largely composed of coarse to fine lapilli, represents most of the mass of the erupted tephra, i.e., about 60 % calculated by using the first four isomass lines (up to the 1,000 g/m^2). Transversally, we observed a central strip characterized by significant mass loading which declined abruptly toward its lateral margins. This mass drop was especially evident thanks to the snow cover underlying the fallout deposit in the summit area; here, a central, thick deposit graded sharply to a discontinuous layer

of scoria clasts laterally, suggesting the presence of strong winds during lava fountaining, which caused a rapid decay of fallout deposit orthogonally to the dispersal axis. Along the dispersal axis, the Main Unit (hence also the CS) becomes discontinuous at distances not much greater than the limit of medial-distal sites.

The Weibull plot (Fig. 9) reproduces well the thinning pattern of the deposit with distance, showing a marked decrease in the first part of the curve followed by a more gradual decay of the mass/area. Figure 4 shows that in the proximal and medial sites the collected samples are poorly sorted and the modes tend to positive values (i.e. smaller grain-sizes) quite rapidly, while samples from distal and very distal sites have unimodal distributions with mode that gradually increases.

Therefore, dispersal data combined with mass/area and grain-size variations prove that the 12–13 January fall deposit was the result of sedimentation from an eruption plume composed, within the first 5–10 km from the vent, of relatively coarse and abundant tephra particles and, in the following, by an eruption plume characterized by a low concentration of fine particles.

Estimated uncertainty of physical parameters

The evaluation of physical parameters characterizing explosive eruptions is affected by uncertainty, mainly related to (a) the representivity of the samples collected from the fall deposit and (b) the use of different methods by different researchers. Limited sampling areas with respect to the whole dispersal area of erupted tephra are largely related to (i) certain geographic features (e.g., volcanoes close to the sea), (ii) the difficulty in approaching the proximal areas due to high volcanic hazard close to the vent or abundant snow cover, and (iii) the lack of sufficient exposures when deposits are eroded and/or buried by successive tephra layers, especially

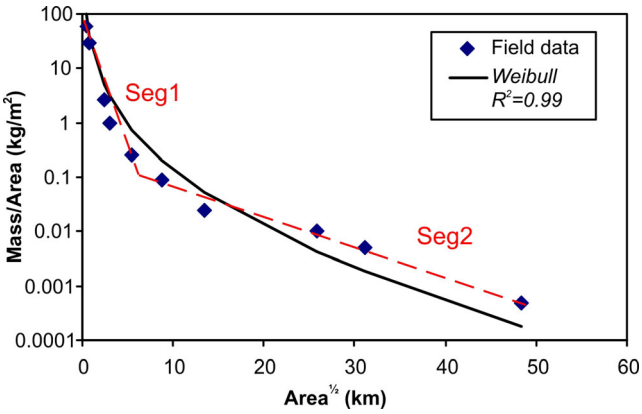

Fig. 9 Semilog plot of mass/area (kg/m^2) versus square root of isomass area (km) showing the Weibull best fit (Bonadonna and Costa 2012)Seg1 and Seg2 indicate particle sedimentation at high and intermediate/low Reynolds numbers, respectively

for ancient eruptions (e.g., Bonadonna and Houghton 2005; Costantini et al. 2009). In the following, we assessed the uncertainty related to the different methodologies for TEM, column height and MER associated to the 12–13 January 2011 lava fountaining, and the uncertainty in the spatial distribution of the tephra samples by analyzing (i) the *whole deposit* between 1 and 103 km from the vent (45 and 38 samples for TEM and TGS, respectively), and (ii) a hypothetical *intermediate deposit* between 6 and 23 km (17 samples).

Concerning the TEM estimation of the *whole deposit*, our research shows that uncertainty due to the different methodologies is about 27 % with respect to the mean value (Table 2). This range is consistent with the differences among TEMs found by Scollo et al. (2007), Pistolesi et al. (2011) and Bonadonna and Costa (2012). In contrast, the TEM (3.4×10^7 kg) calculated from a partial set of samples, when the tephra deposit covers the east sector alone, is much smaller, only ~1/5 of the TEM (1.49×10^8 kg) of the whole deposit (Table 2). Hence, the TEM produced from the hypothetical *intermediate deposit* alone is a substantial underestimate of that calculated for the *whole deposit*; the reduction is mainly due to the lack of the proximal samples.

The lack of proximal samples may cause even greater differences for the calculated TGS. The Voronoi method is significantly affected by the sample distribution generally, and by very proximal samples (Bonadonna and Houghton 2005). Figure 8 shows a discrepancy between the *whole* and hypothetical *intermediate* deposits and also a different shape of the grain-size distribution. This concurs with the study of Bonadonna and Houghton (2005) who demonstrated that the calculated distribution depends strongly on the goodness of the datasets. The *whole deposit* is coarser and characterized by an asymmetric curve shifted towards the coarse particles; conversely, the hypothetical *intermediate deposit* is composed mostly of fine particles (0 and 1 phi). The latter distribution implies that a lava fountain from Etna may generate a rather well-sorted tephra deposit, thus providing an erroneous assessment of the real fragmentation processes governing the eruptive style. Furthermore, the Opening Unit layer, due to its limited extent and mass, has negligible effect on the TGS of the *whole deposit*.

We also found significant differences in the column height estimation. From the determination of the largest clast sizes of the fallout deposit, we obtained column height estimates of between 6.8 and 13.8 km above the vent (Carey and Sparks 1986) (Table 5). The column height calculated using Wilson and Walker (1987), Mastin et al. (2009) and Pistolesi et al. (2011) methods gave lower values than the results calculated with the Carey and Sparks (1986) method. The lower estimation (6.8 km) from the Carey and Sparks (1986) method is consistent with the height of 6 km above the vent obtained by video-recording analysis by Calvari et al. (2011). However, considering a 6-km-high eruption column, we should have a

MER of ~10^5 kg/s (calculated using the equations from Table 5), which is at least an order of magnitude greater than the value of ~10^4 kg/s provided by the TEM of the deposit (Table 2) and the well-constrained duration of the eruption.

We suggest that the difference between these two MERs could depend on the following points:

a. The height values estimated from the mean value of the MER (Table 2) and the equations from Table 5, represent a time-averaged value of the entire *paroxysmal phase*; consequently, we calculate the time-averaged MER, when an instantaneous MER could be greater. Conversely, the plume height provided from both video-recordings and the Carey and Sparks method (lower value) gives an estimate of the instantaneous magma discharge, i.e. 10^5 kg/s, hence an overestimation of the average MER. Furthermore, the Carey and Sparks (1986) method bears an intrinsic uncertainty of at least ± 20 % (Biass and Bonadonna 2011) and differences could also be due to the fact that this method has been proposed for Plinian eruptions, so that its application to lava fountains should be made with caution;
b. Similarly, the pulsating nature of the lava fountaining activity may cause fluctuations in magma jets, more evident at the beginning and end of the paroxysmal activity causing a variation of the plume height with time;
c. Plume structure and content: potential of plume height to vary as a function of different factors, such as the concentration of gas/water vapor with respect to eruption products in the convective plume, and the thermal contribution of the larger clasts inside the lava fountain (Stothers et al. 1986);
d. The column height value obtained by video-recordings from Calvari et al. (2011), which could have considerable uncertainty because the volcanic plume moved toward the camera used for their estimation, whereas good measurements are obtained when the plume blows perpendicular to the field of view (Scollo et al. 2014);
e. Finally, it should be highlighted that in order to evaluate the column height by the Carey and Sparks (1986) method, we used the mean value of the maximum length instead of the mean value of the three axes of the largest clasts, which could cause overstimation of the column height. On the other hand, we do not take into consideration that the measured scoria could be partially broken on impact with the ground.

Eruption dynamics

The study of the 12–13 January 2011 lava fountain has enabled improvement in our knowledge of Etna lava fountain eruption dynamics. For this specific event, we found that the transition between *resumption* and *paroxysmal* phases, typically characterized by the sharp evolution from Strombolian to lava fountaining activity, may be preceded and/or accompanied by the deposition of a small, rarely quantified, tephra deposit in the proximal area (Opening Unit).

A quantitative assessment of the fall deposit (Main Unit) shows that more than 60 % of the TEM emplaced during the *paroxysmal phase* covered an area that is only 0.4 % of the whole dispersal area (8.7 km^2 vs. ~2,350 km^2) and is confined to within the first 5–6 km from the eruptive vent. Furthermore, on the basis of the TGS distribution, 84 % of the particles composing the fall deposit are coarser than 0 phi (i.e., larger than 1 mm), while conversely only less than 3 % of ash grains smaller than 2 phi (i.e., <0.125 mm) fell on Sicily. These data thus show that the tephra fall produced from the 12–13 January lava fountain and deposited on Sicily was coarse and composed of a negligible amount of fine ash. The 12–13 January event may be considered as a typical lava fountain at Etna, during which magma rise and fragmentation processes develop <10-km-height eruption plumes above the vent (Scollo et al. 2014) and cause sedimentation of coarse scoria and lapilli particles within a few kilometers from the vent. Minor amounts of ash particles are dispersed for up to tens of kilometers away.

The presence of different regimes of particle sedimentation during the 12–13 January lava fountain may be highlighted by drawing, on the mass/area versus area$^{1/2}$ plot, two distinct segments (Fig. 9). The first steep segment (Seg1) approximately corresponds to the proximal and medial deposits, while the second, lower-slope segment represents the distal and very distal deposits. The observed break-in-slope would reflect the change in tephra fallout from different sedimentation regimes (Bonadonna et al. 1998). We infer that Seg1 includes the deposit produced by the column margins plus the tephra falling from the initial part of the umbrella region, i.e., the one characterized by the deposition of high Reynolds number particles. Seg2 is inferred to represent the deposit of finer-grained particles with intermediate and low Reynolds numbers and characterized by lower thinning with increasing distance from the vent.

It is well known that most of the eruptive processes occurring during lava fountaining begin in the conduit and control the lava fountain dynamic structure, as defined by Head and Wilson (1989), who distinguished an outer portion of the fountain from an inner portion. For example, friction along the conduit walls would act to lower magma ascent velocity and thus lower velocity and temperature on outer jet margins, resulting in a different magma fragmentation efficiency than in the inner conduit, i.e. greater particles (in size) will be produced on outer jet margins. Conversely, most of the fountaining magma is erupted from the inner conduit, so lava fountains have clasts which are hotter for longer with respect to that from the conduit margins, and the greater available heat enhances the convection process to produce increased plume heights. The combination of such processes

may ultimately lead to the zonation of the volcanic plume as reflected in the central strip observed in the fall deposit. In addition, a small spread angle of erupted tephra is expected in a relatively narrow conduit, probably like the one formed during the 12–13 January episode at SEC (where the last lava fountaining occurred in 2008), and the width of the outer fountain should also be substantial with respect to the width of the inner fountain.

Conclusions

The reconstruction of the 12–13 January tephra fall deposit enables us to understand the representativity of collected samples and evaluate the uncertainty in estimated physical parameters (TEM, TGS, MER and column height). Our study shows that the analysis of a partial set of samples may misrepresent physical parameters of a fall deposit, and that caution is needed when assessing the eruptive processes associated with tephra fallout from Etna (as well as for other volcanoes). In fact, inferring a TEM using only *intermediate deposits*, representing only a portion of the total deposit, could lead to a considerable uncertainty. Concerning the TGS distributions calculated using the Voronoi method seem to be shifted toward lower grain-size when proximal, coarse samples are lacking, at least for fall deposits from lava fountains of Etna.

Understanding whether these are systematic differences between the TEM, TGS and column heights calculated for a *whole deposit* versus an *intermediate deposit* is a desirable and useful goal to improve the monitoring of explosive activity at Etna. Indeed, this understanding is crucial for work at very active volcanoes, like Etna, because results from these volcanoes are widely used as input parameters to volcanic ash dispersal models used for assessing potential hazard to air traffic and to mitigate related risks.

In the future, new techniques for estimating from fall deposits the TGS and column height of basaltic eruptions with eruption columns less than 10 km in height are needed.

Acknowledgments We especially wish to thank F. Ciancitto, M. Coltelli, S. Di Stefano, L. Lodato and G. Spata for collaboration during field survey and sample collection. E. De Beni and C. Proietti contributed greatly to the cartographic elaborations. We are also indebted to S. Conway for revising the English language of the text. C. Bonadonna and R. Cioni are acknowledged for their helpful suggestions during the final version of the paper. We also thank the Executive Editor Prof. James D. L. White, the Associate Editor Prof. Thorvaldur Thordarson, Dr. Rebecca Carey and an anonymous reviewer for closely and constructively reviewing the paper.

References

Allard P, Burton M, Murè F (2005) Spectroscopic evidence for a lava fountain driven by previously accumulated magmatic gas. Nature 433:407–410

Allard P, Behncke B, D'Amico S, Neri M, Gambino S (2006) Mount Etna 1993–2005: anatomy of an evolving eruptive cycle. Earth Sci Rev 78:85–114. doi:10.1016/j.earscirev.2006.04.002

Alparone S, Andronico D, Lodato L, Sgroi T (2003) Relationship between tremor and volcanic activity during the Southeast Crater eruption on Mount Etna in early 2000. J Geophys Res 108: B52241. doi:10.1029/2002JB001866

Alparone S, Andronico D, Sgroi T, Ferrari F, Lodato L, Reitano D (2007) Alert system to mitigate tephra fallout hazards at Mt. Etna Volcano, Italy. Nat Hazards 43:333–350

Andronico D, Corsaro RA (2011) Lava fountains during the episodic eruption of South-East Crater (Mt. Etna), 2000: insights into magma-gas dynamics within the shallow volcano plumbing system. Bull Volcanol 73(9):1165–1178. doi:10.1007/s00445-011-0467-y

Andronico D, Cristaldi A, Scollo S (2008a) The 4–5 September 2007 lava fountain at South-East Crater of Mt Etna, Italy. J Volcanol Geotherm Res 173:325–328

Andronico D, Scollo S, Cristaldi A, Caruso S (2008b) The 2002–03 Etna explosive activity: tephra dispersal and features of the deposit. J Geophys Res 113:B04209. doi:10.1029/2007JB005126

Andronico D, Scollo S, Cristaldi A, Ferrari F (2009a) Monitoring ash emission episodes at Mt. Etna: the 16 November 2006 case study. J Volcanol Geotherm Res 180(2–4):123–134. doi:10.1016/j.jvolgeores.2008.10.019

Andronico D, Spinetti C, Cristaldi A, Buongiorno MF (2009b) Observations of Mt. Etna volcanic ash plumes in 2006: an integrated approach from ground-based and polar satellite NOAA-AVHRR monitoring system. J Volcanol Geotherm Res. doi:10.1016/j.jvolgeores.2008.11.013

Andronico D, Cristaldi A, Ferrari F, Jauvin M, Lo Castro MD, Scollo S (2012) Etnean lava fountains: insights into the 2011–12 sequence. Proceedings of Cities on Volcanoes 7, Colima (Mexico), 19–23 November 2012

Andronico D, Lo Castro MD, Sciotto M, Spina L (2013) The 2010 ash emissions at the summit craters of Mt Etna: relationship with seismo-acoustic signals. J Geophys Res 118:51–70. doi:10.1029/2012JB009895

Andronico D, Scollo S, Lo Castro MD, Cristaldi A, Lodato L, Taddeucci J (2014) Eruption dynamics and tephra dispersal from the 24 November 2006 paroxysm at South-East Crater, Mt Etna, Italy. 274 (2014) 78–91 doi:10.1016/j.jvolgeores.2014.01.009

Barberi F, Coltelli M, Frullani A, Rosi M, Almeida E (1995) Chronology and dispersal characteristics of recently (last 5000 years) erupted tephra of Cotopaxi (Ecuador): implications for long term eruptive forecasting. J Volcanol Geotherm Res 69:217–239

Barsotti S, Andronico D, Neri A, Del Carlo P, Baxter PJ, Aspinall WP, Hincks T (2010) Quantitative assessment of volcanic ash hazards for health and infrastructure at Mt. Etna (Italy) by numerical simulation. J Volcanol Geotherm Res 192(1–2):85–96. doi:10.1016/j.jvolgeores.2010.02.011

Behncke B, Neri M, Pecora E, Zanon V (2006) The exceptional activity and growth of the Southeast Crater, Mount Etna (Italy), between 1996 and 2001. Bull Volcanol 69(2):149–173. doi:10.1007/s00445-006-0061-x

Behncke B, Branca S, Corsaro RA, De Beni E, Miraglia L, Proietti P (2014) The 2011–2012 summit activity of Mount Etna: birth, growth and products of the new SE crater. J Volcanol Geotherm Res 270:10–21

Biass S, Bonadonna C (2011) A quantitative uncertainty assessment of eruptive parameters derived from tephra deposits: the example of

two large eruptions of Cotopaxi volcano, Ecuador. Bull Volcanol 73:73–90Bonadonna C, Houghton BF (2005) Total grain-size distribution and volume of tephra-fall deposits. Bull Volcanol 67:441–456

Bonadonna C, Costa A (2012) Estimating the volume of tephra deposits: a new simple strategy. Geology 40:415–418. doi:10.1130/G32769.1

Bonadonna C, Houghton BF (2005) Total grain-size distribution and volume of tephra-fall deposits. Bull Volcanol 67:441–456

Bonadonna C, Cioni R, Pistolesi M, Connor C, Scollo S, Pioli L, Rosi M (2013) Determination of the largest clast sizes of tephra deposits for the characterization of explosive eruptions: a study of the IAVCEI commission on tephra hazard modeling. Bull Volcanol 75(1):1–15. doi:10.1007/s00445-012-0680-3

Bonadonna C, Ernst GGJ, Sparks RSJ (1998) Thickness variations and volume estimates of tephra fall deposits: the importance of particle Reynolds number. J Volcanol Geotherm Res 81:173–187

Calvari S, Salerno GG, Spampinato L, Gouhier M, La Spina A, Pecora E, Harris AJL, Labazuy P, Biale E, Boschi E (2011) An unloading foam model to constrain Etna's 11–13 January 2011 lava fountaining episode. J Geophys Res 116:B11207. doi:10.1029/2011JB008407

Carey SN, Sparks RSJ (1986) Quantitative models of the fallout and dispersal of tephra from volcanic eruption columns. Bull Volcanol 48:109–125

Costantini L, Bonadonna C, Houghton BF, Wehrmann H (2009) New physical characterization of the Fontana lapilli basaltic Plinian eruption, Nicaragua. Bull Volcanol 71:337–355. doi:10.1007/s00445-008-0227-9

Falsaperla S, Alparone S, D'Amico S, Di Grazia G, Ferrari F, Langer H, Sgroi T, Spampinato S (2005) Volcanic Tremor at Mt. Etna, Italy, Preceding and Accompanying the Eruption of July–August, 2001. Pure Appl Geophys 162(12):2111–2132. doi:10.1007/s00024-005-2710-y, 0033-4553/05/112111-22

Fierstein J, Nathenson M (1992) Another look at the calculation of fallout tephra volumes. Bull Volcanol 54:156–167

Folk RL, Ward WC (1957) Brazos River bar: a study in the significance of grain size parameters. J Sediment Petrol 27:3–26

Ganci G, Harris AJL, Del Negro C, Guehenneux Y, Cappello A, Labazuy P, Calvari S, Gouhier M (2012) A year of lava fountaining at Etna: volumes from SEVIRI. Geophys Res Lett 39:L06305. doi:10.1029/2012GL051026

Head JW III, Wilson L (1989) Basaltic pyroclastic erutions: influence of gas-release patterns and volume fluxes on fountain structure, and the formation of cinder cones, spatter cones, rootless flows, lava ponds and lava flows. J Volcanol Geotherm Res 37:261–271

Inman DL (1952) Measures for describing the size distribution of sediments. J Sediment Petrol 22:125–145

Lo Castro MD, Andronico D (2008) Operazioni di base per la misura della distribuzione granulometrica di particelle vulcaniche tramite il CAMSIZER. Rapporti Tecnici INGV 79:1–35

Longchamp C, Bonadonna C, Bachmann O, Skopelittis A (2011) Characterization of tephra deposits with limited exposure: the example of the two largest explosive eruptions at Nisyros volcano (Greece). Bull Volcanol 73:1337–1352. doi:10.1007/s00445-011-0469

Mastin LG, Guffanti M, Servranckx R, Webley P, Barsotti S, Dean K, Durant A, Ewert JW, Neri A, Rose WI, Schneider D, Siebert L, Stunder B, Swanson G, Tupper A, Volentik A, Waythomas CF (2009) A multidisciplinary effort to assign realistic source parameters to models of volcanic ash-cloud transport and dispersion during eruptions. J Volcanol Geotherm Res 186:10–21. doi:10.1016/j.jvolgeores.2009.10.013

Newhall CG, Self S (1982) The volcanic explosivity index (VEI): an estimate of explosive magnitude for historical volcanism. J Geophys Res 87(C2):1231–1238

Parfitt EA, Wilson L (1994) The 1983–86 Pu'u'O'o eruption at Kilauea Volcano, Hawaii: a study of dike geometry and eruption mechanisms for a long-lived eruption. J Volcanol Geotherm Res 59:179–205

Pistolesi M, Rosi M, Cioni R, Cashman KV, Rossotti A, Aguilera E (2011) Physical volcanology of the post-twelfth-century activity at Cotopaxi volcano, Ecuador: behavior of an andesitic central volcano. Geol Soc Am Bull 123(5–6):1193–1215. doi:10.1130/B30301.1

Polacci M, Corsaro R, Andronico D (2006) Coupled textural and compositional characterization of basaltic scoria: Insights into the transition from Strombolian to fire fountain activity at Mount Etna, Italy. Geology 34(3):201–204. doi:10.1130/G223181.1

Pyle DM (1989) The thickness, volume and grain size of tephra fall deposits. Bull Volcanol 51:1–15

Pyle DM (1995) Assessment of the minimum volume of tephra fall deposits. J Volcanol Geotherm Res 69:379–382

Rose WI (1993) Comment on another look at the calculation of fallout tephra volumes. Bull Volcanol 55:372–374

Scollo S, Del Carlo P, Coltelli M (2007) Tephra fallout of 2001 Etna flank eruption: analysis of the deposit and plume dispersion. J Volcanol Geotherm Res 160:147–164

Scollo S, Folch A, Costa A (2008) A parametric and comparative study of different tephra fallout models. J Volcanol Geotherm Res 176:199–211

Scollo S, Coltelli M, Bonadonna, Del Carlo P (2013) Tephra hazard assessment at Mt. Etna (Italy). Nat Hazards Earth Syst Sci Discuss 1:2945–2981. doi:10.5194/nhessd-1-2945-2013

Scollo S, Prestifilippo M, Pecora E, Corradini S, Merucci L, Spata G, Coltelli M (2014) Eruption Column Height Estimation of the 2011–2013 Etna lava fountains. Ann Geophys, in print

Stothers RB, Wolff JA, Self S, Rampino MR (1986) Basaltic fissure eruptions, plume heights, and atmospherical aerosols. Geophys Res Lett 13:725–728

Walker GPL (1971) Grain-size characteristic of pyroclastic deposits. J Geol 79:696–714

Wilson L, Walker GPL (1987) Explosive volcanic eruptions: VI. Ejecta dispersal in Plinian eruptions: the control of eruption condition and atmospheric properties. Geophys J R Astron Soc 89:657–679